Band modulation and in-plane propagation of surface plasmons in composite nanostructures

Di-Hu Xu, Kun Zhang, Ming-Rui Shao, Hong-Wei Wu, Ren-Hao Fan, Ru-Wen Peng,* and Mu Wang

National Laboratory of Solid State Microstructures and Department of Physics, National Center of Microstructures and Quantum Manipulation, Nanjing University, Nanjing 210093, China
rwpeng@nju.edu.cn

Abstract: In this work, we have experimentally and theoretically studied band modulation and in-plane propagation of surface plasmons (SPs) in composite nanostructures with aperture arrays and metallic gratings. It is shown that the plasmonic band structure of the composite system can be significantly modulated because of coupling between the aperture and grating. By changing the relative positions between these optical components, the resonant modes would shift or split. And the resonant SP modes launched on the structure surface can be effectively modified by the geometric parameters. Further, we provide an experimental observation to directly show the SP in-plane propagation by using far-field measurements, which agree with the simulated results. Our study offers a convenient way for observing the SP propagation in far field, and provides unique composite nanostructures for possible applications in subwavelength optodevices, such as optical sensors and detectors.

©2014 Optical Society of America

OCIS codes: (250.5403) Plasmonics;.(240.0240) Optics at surfaces; (290.0290) Scattering.

References and links

1. R. H. Ritchie, "Plasma losses by fast electrons in thin films," Phys. Rev. **106**(5), 874–881 (1957).
2. K. Kneipp, Y. Wang, H. Kneipp, L. T. Perelman, I. Itzkan, R. R. Dasari, and M. S. Feld, "Single molecule detection using surface-enhanced Raman scattering (SERS)," Phys. Rev. Lett. **78**(9), 1667–1670 (1997).
3. W. L. Barnes, A. Dereux, and T. W. Ebbesen, "Surface plasmon subwavelength optics," Nature **424**(6950), 824–830 (2003).
4. A. V. Zayats, I. I. Smolyaninov, and A. A. Maradudin, "Nano-optics of surface plasmon polaritons," Phys. Rep. **408**(3–4), 131–314 (2005).
5. N. Fang, H. Lee, C. Sun, and X. Zhang, "Sub-diffraction-limited optical imaging with a silver superlens," Science **308**(5721), 534–537 (2005).
6. E. Ozbay, "Plasmonics: merging photonics and electronics at nanoscale dimensions," Science **311**(5758), 189–193 (2006).
7. S. Kim, J. Jin, Y.-J. Kim, I.-Y. Park, Y. Kim, and S.-W. Kim, "High-harmonic generation by resonant plasmon field enhancement," Nature **453**(7196), 757–760 (2008).
8. R. F. Oulton, V. J. Sorger, T. Zentgraf, R. M. Ma, C. Gladden, L. Dai, G. Bartal, and X. Zhang, "Plasmon lasers at deep subwavelength scale," Nature **461**(7264), 629–632 (2009).
9. H. Raether, *Surface Plasmons on Smooth and Rough Surfaces and on Gratings* (Springer, 1988).
10. T. W. Ebbesen, H. J. Lezec, H. F. Ghaemi, T. Thio, and P. A. Wolff, "Extraordinary optical transmission through sub-wavelength hole arrays," Nature **391**(6668), 667–669 (1998).
11. L. Martín-Moreno, F. J. García-Vidal, H. J. Lezec, K. M. Pellerin, T. Thio, J. B. Pendry, and T. W. Ebbesen, "Theory of extraordinary optical transmission through subwavelength hole arrays," Phys. Rev. Lett. **86**(6), 1114–1117 (2001).
12. H. J. Lezec, A. Degiron, E. Devaux, R. A. Linke, L. Martin-Moreno, F. J. Garcia-Vidal, and T. W. Ebbesen, "Beaming light from a subwavelength aperture," Science **297**(5582), 820–822 (2002).
13. Z. Ruan and M. Qiu, "Enhanced transmission through periodic arrays of subwavelength holes: the role of localized waveguide resonances," Phys. Rev. Lett. **96**(23), 233901 (2006).
14. H. Liu and P. Lalanne, "Microscopic theory of the extraordinary optical transmission," Nature **452**(7188), 728–731 (2008).
15. Y. J. Bao, R. W. Peng, D. J. Shu, M. Wang, X. Lu, J. Shao, W. Lu, and N. B. Ming, "Role of interference between localized and propagating surface waves on the extraordinary optical transmission through a

#217826 - $15.00 USD Received 25 Jul 2014; revised 5 Oct 2014; accepted 8 Oct 2014; published 14 Oct 2014

subwavelength-aperture array," Phys. Rev. Lett. **101**(8), 087401 (2008).
16. F. J. Garcia-Vidal, L. Martin-Moreno, T. W. Ebbesen, and L. Kuipers, "Light passing through subwavelength apertures," Rev. Mod. Phys. **82**(1), 729–787 (2010).
17. D. Crouse and P. Keshavareddy, "Polarization independent enhanced optical transmission in one-dimensional gratings and device applications," Opt. Express **15**(4), 1415–1427 (2007).
18. F. López-Tejeira, F. J. García-Vidal, and L. Martín-Moreno, "Scattering of surface plasmons by one-dimensional periodic nanoindented surfaces," Phys. Rev. B **72**(16), 161405 (2005).
19. M. U. Gonzalez, J.-C. Weeber, A.-L. Baudrion, A. Dereux, A. L. Stepanov, J. R. Krenn, E. Devaux, and T. W. Ebbesen, "Design, near-field characterization, and modeling of 45° surface-plasmon Bragg mirrors," Phys. Rev. B **73**(15), 155416 (2006).
20. F. Lopez-Tejeira, S. G. Rodrigo, L. Martin-Moreno, F. J. Garcia-Vidal, E. Devaux, T. W. Ebbesen, J. R. Krenn, I. P. Radko, S. I. Bozhevolnyi, M. U. Gonzalez, J. C. Weeber, and A. Dereux, "Efficient unidirectional nanoslit couplers for surface plasmons," Nat. Phys. **3**(5), 324–328 (2007).
21. J.-C. Weeber, J. R. Krenn, A. Dereux, B. Lamprecht, Y. Lacroute, and J. P. Goudonnet, "Near-field observation of surface plasmon polariton propagation on thin metal stripes," Phys. Rev. B **64**(4), 045411 (2001).
22. S. I. Bozhevolnyi, J. Erland, K. Leosson, P. M. W. Skovgaard, and J. M. Hvam, "Waveguiding in surface plasmon polariton band gap structures," Phys. Rev. Lett. **86**(14), 3008–3011 (2001).
23. B. Wang and G. P. Wang, "Plasmon Bragg reflectors and nanocavities on flat metallic surfaces," Appl. Phys. Lett. **87**(1), 013107 (2005).
24. H. Leong and J. Guo, "A surface plasmon resonance spectrometer using a super-period metal nanohole array," Opt. Express **20**(19), 21318–21323 (2012).
25. D. W. Pohl, W. Denk, and M. Lanz, "Optical stethoscopy: image recording with resolution λ/20," Appl. Phys. Lett. **44**(7), 651–653 (1984).
26. A. Lewis, M. Isaacson, A. Harootunian, and A. Muray, "Development of a 500 Å spatial resolution light microscope," Ultramicroscopy **13**(3), 227–231 (1984).
27. D. S. Kim, S. C. Hohng, V. Malyarchuk, Y. C. Yoon, Y. H. Ahn, K. J. Yee, J. W. Park, J. Kim, Q. H. Park, and C. Lienau, "Microscopic origin of surface-plasmon radiation in plasmonic band-gap nanostructures," Phys. Rev. Lett. **91**(14), 143901 (2003).
28. H. Ditlbacher, A. Hohenau, D. Wagner, U. Kreibig, M. Rogers, F. Hofer, F. R. Aussenegg, and J. R. Krenn, "Silver nanowires as surface plasmon resonators," Phys. Rev. Lett. **95**(25), 257403 (2005).
29. A. Drezet, A. Hohenau, A. L. Stepanov, H. Ditlbacher, B. Steinberger, N. Galler, F. R. Aussenegg, A. Leitner, and J. R. Krenn, "How to erase surface plasmon fringes," Appl. Phys. Lett. **89**(9), 091117 (2006).
30. L. Li, T. Li, S. M. Wang, C. Zhang, and S. N. Zhu, "Plasmonic Airy beam generated by in-plane diffraction," Phys. Rev. Lett. **107**(12), 126804 (2011).
31. S. Zhang, H. Wei, K. Bao, U. Håkanson, N. J. Halas, P. Nordlander, and H. Xu, "Chiral surface plasmon polaritons on metallic nanowires," Phys. Rev. Lett. **107**(9), 096801 (2011).
32. H. Wei, Z. Li, X. Tian, Z. Wang, F. Cong, N. Liu, S. Zhang, P. Nordlander, N. J. Halas, and H. Xu, "Quantum dot-based local field imaging reveals plasmon-based interferometric logic in silver nanowire networks," Nano Lett. **11**(2), 471–475 (2011).
33. S. J. Pennycook and C. Colliex, "Spectroscopic imaging in electron microscopy," MRS Bull. **37**(1), 13–18 (2012).
34. D. Rossouw and G. A. Botton, "Plasmonic response of bent silver nanowires for nanophotonic subwavelength waveguiding," Phys. Rev. Lett. **110**(6), 066801 (2013).
35. A. Taflove and S. C. Hagness, *Computational Electrodynamics: The Finite-Difference Time-Domain Method* (Artech House, 2000).
36. A. D. Rakic, A. B. Djurisic, J. M. Elazar, and M. L. Majewski, "Optical properties of metallic films for vertical-cavity optoelectronic devices," Appl. Opt. **37**(22), 5271–5283 (1998).
37. E. D. Palik, *Handbook of Optical Constants of Solids* (Academic, 1998).
38. Q. Cao and P. Lalanne, "Negative role of surface plasmons in the transmission of metallic gratings with very narrow slits," Phys. Rev. Lett. **88**(5), 057403 (2002).
39. Z. H. Tang, R. W. Peng, Z. Wang, X. Wu, Y. J. Bao, Q. J. Wang, Z. J. Zhang, W. H. Sun, and M. Wang, "Coupling of surface plasmons in nanostructured metal/dielectric multilayers with subwavelength hole arrays," Phys. Rev. B **76**(19), 195405 (2007).
40. M. G. Moharam, E. B. Grann, D. A. Pommet, and T. K. Gaylord, "Formulation for stable and efficient implementation of the rigorous coupled-wave analysis of binary gratings," J. Opt. Soc. Am. A **12**(5), 1068–1076 (1995).
41. R. Petit, *Electromagnetic Theory of Gratings* (Spinger-Verlag, 1980).
42. C. Sauvan, P. Lalanne, J. C. Rodier, J. P. Hugonin, and A. Talneau, "Accurate modeling of line-defect photonic crystal waveguides," IEEE Photon. Technol. Lett. **15**(9), 1243–1245 (2003).

1. Introduction

Surface plasmons (SPs) are essentially the collective charge density waves existing at the metal-dielectric interface, which have attracted much attention for their unique properties, such as breaking the diffraction limit and field enhancement at the interface [1–8]. As we know, SPs

#217826 - $15.00 USD Received 25 Jul 2014; revised 5 Oct 2014; accepted 8 Oct 2014; published 14 Oct 2014
(C) 2014 OSA

are so sensitive to the interface [9] that designed nanostructures could effectively modulate the excitation and propagation of SPs, and the interactions between SPs and nanostructures can lead to various interesting effects. For instance, in the periodic nanoaperture array on a metal film, surface plasmon resonance can enhance the light transmission through this structured metal film, which was first reported as the extraordinary optical transmission (EOT) phenomenon in 1998 [10] and then widely studied in recent years [11–17]. In structures with periodic metal gratings, the propagating SPs can be greatly reflected at the frequencies in the band gap [18–20], and such structures could be utilized as Bragg reflectors. Other well-designed gratings may significantly modulate the properties of SP propagation, such as the propagation direction and the energy transport [21–23].

By combining aperture arrays and gratings, one can tune the surface plasmon resonance in the aperture arrays using the gratings. For example, a super-period nanohole array grating, which leads to resonance mode splitting under polarized incident light [24], provides one method for combining aperture arrays and gratings. Here, we offer another method by designing composite structures that inlay periodic gratings into aperture arrays. The coupling in the composite structures can be tuned by changing the relative displacement between the aperture arrays and the gratings, which also results in the surface plasmon resonance mode splitting.

Because the surface plasmons propagate at the metal-dielectric interface, it is difficult to experimentally track the propagation of SPs. One direct way to map the surface plasmon field uses a near-field technique such as scanning near-field optical microscopy (SNOM) [25–28]. Furthermore, there are indirect ways to study the SPs propagation in far-field, such as by leakage radiation microscopy [29,30], quantum dot imaging [31,32], and electron energy loss spectroscopy (EELS) [33,34], which mostly involve observational measurements. Here, we report a semi-quantitative measurement method, using a charge coupled-device (CCD) camera to map the far field image and measure the field intensity coupled out by a groove. The captured far-field distributions are in good agreement with the simulation results. Moreover, the out-coupled field intensities are also in accordance with the calculated intensities. Thus, this method can be used to study the propagating properties of SPs.

2. Optical properties of the composite structures

We first consider systems consisting of only an aperture array or a metallic grating, as respectively illustrated in Figs. 1(a) and 1(c). Figure 1(a) schematically shows an aperture array in 100 nm thick silver film on the silicon substrate, with an aperture diameter d = 150 nm and an array period of $P_x = P_y = P_1 = 540$ nm. Here, we use a commercial finite-difference time-domain (FDTD) [35] software package (Lumerical FDTD Solutions) to perform the simulations, where the frequency-dependent permittivity of Ag is obtained from the Lorentz-Drude model [36] and the permittivity of Si is obtained from Palik [37]. Figure 1(b) exhibits the calculated reflection spectrum of the aperture array under normal incidence, with a resonant dip at 575 nm. By applying the phase-match condition for converting the free-space waves into SPs at the air-silver interface, the corresponding resonant wavelength for the fundamental resonant mode can be expressed approximately as $\lambda_{re} \cong P_1 \cdot \mathrm{Re}\{[\varepsilon_d \cdot \varepsilon_m / (\varepsilon_d + \varepsilon_m)]^{1/2}\}$ [38], where ε_d and ε_m are the permittivity of dielectric and metal, respectively. In this way, we find λ_{re} = 568 nm for this system, which reasonably agrees with the simulated results. We label the mode at the dip of the reflection spectrum as mode *A*(1,0) as indicated in our previous work [39].

#217826 - $15.00 USD Received 25 Jul 2014; revised 5 Oct 2014; accepted 8 Oct 2014; published 14 Oct 2014
(C) 2014 OSA

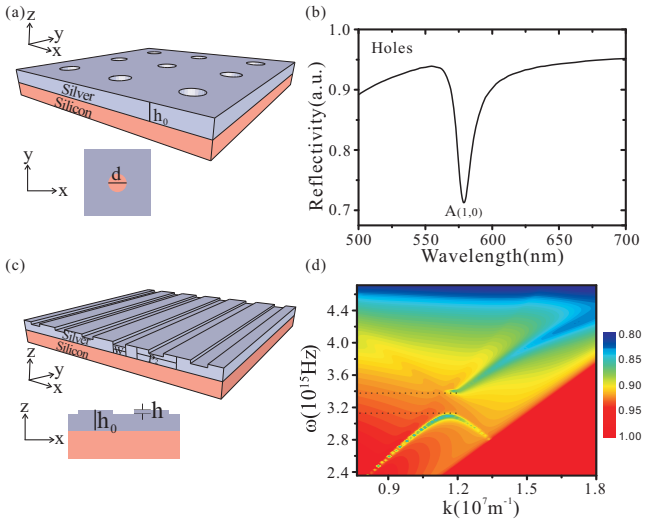

Fig. 1. The schematic of (a) an aperture array and (c) a grating in the silver film. (b) The reflection spectrum of the aperture array under normal incidence. (d) The calculated plasmonic band structure of the grating for TM light.

Figure 1(c) schematically describes the metallic grating in 100nm-thick silver film on the silicon substrate, with the groove width of W = 100 nm, grating period of P_2 = 270 nm, and groove depth of h = 20 nm. To obtain the plasmonic band structure in the grating, we employ the rigorous coupled-wave analysis (RCWA) method [40] to calculate the reflectance of the grating at different oblique incident angles. Figure 1(d) shows the plasmonic band structure in the grating when the electric field of the incident light lies along the *x*-direction, *i.e.*, transverse magnetic (TM) light. The band structure shows an obvious gap in the 560 - 600 nm wavelength range, which is marked by a dotted line. Actually similar results for band structures of gratings have been achieved by relying on some well-developed theoretical formalisms, such as the pology. The pology [41,42], where the optical modes are computed as the complex poles of a transversal scattering matrix that links the electromagnetic field amplitude in the claddings, has been successfully applied to study diffraction anomalies or resonances, and even the Bloch modes of photonic crystal waveguides [42]. In our design, the SP resonant mode launched in the aperture array falls in the band gap region of the grating. Next we will demonstrate that introducing gratings into the aperture arrays can modulate band structures.

When the grating is introduced into the aperture array as described in Fig. 2(a), we mark the relative displacement between them with X, which represents the nearest relative position between an aperture center and a groove center. For example, When the aperture center coincides with the groove center, we set X = 0. The normally incident light with the electric field polarized along the *x*-direction corresponds to TM light, while transverse electric (TE) light corresponds to an electric field polarized along the *y*-direction. We then use the FDTD method to study the optical properties of composite structures with different X, where the boundary conditions are periodic in both the *x*- and *y*-direction.

#217826 - $15.00 USD Received 25 Jul 2014; revised 5 Oct 2014; accepted 8 Oct 2014; published 14 Oct 2014
(C) 2014 OSA

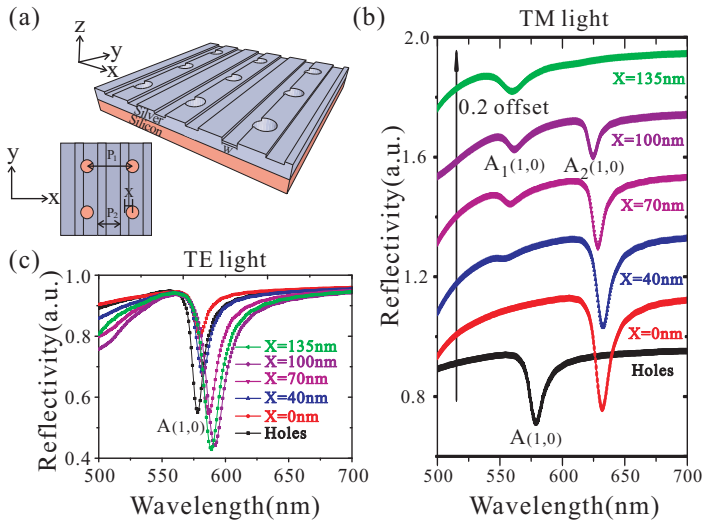

Fig. 2. The schematic of (a) the composite structure. The calculated reflection spectra under normal incidence for (b) TM polarization light and (c) TE polarization light.

Figure 2(b) shows the simulated reflection spectra under TM light illumination, where the black line presents the reflection spectrum of the aperture array without gratings, and the other lines, which are offset for clarification, are spectra of the composite structures with different relative positions. For the X = 0 case, the resonant dip has an obvious red shift compared with the initial case without gratings, this shift is a result of the coupling between the aperture array and the grating. When the relative position X increases, two resonant dips emerge in the reflection spectra, as the basic mode A(1,0) splits gradually into two modes. The left mode is labeled $A_1(1,0)$, while the right mode is labeled $A_2(1,0)$. When X increases from 40 nm to 100 nm (as shown in Fig. 2(b)), $A_1(1,0)$ has a red shift, while $A_2(1,0)$ has a blue shift. Furthermore, as X increases to 135nm, there is only one resonant dip again, that has an obvious blue shift compared with the initial case without gratings. In contrast, under the TE light illumination, only one resonant dip occurs in all cases (as shown in Fig. 2(c)). Therefore, we focus our attention on cases with TM incident light.

To obtain detailed insight into the resonant modes under TM light illumination, we have calculated the electric field intensity distributions at the resonant mode on the surface of the structures. Figure 3(a) shows the reflection spectrum of the aperture array under normal incidence, with a resonant dip at 575 nm indicating the basic mode A(1,0). The corresponding electric field intensity distribution at 575 nm is shown in Fig. 3(d), where the electric field is primarily localized in the hole and distributes as a dipole. For the composite structure with X = 0, the resonant mode shifts to 632 nm as shown in Fig. 3(b), and the corresponding electric field intensity distribution at the resonant wavelength is shown in Fig. 3(e). The electric field is primarily distributed on the edge of the neighbouring groove far from the aperture, while a small electric field is localized in the aperture, corresponding with the resonant redshift in the spectrum. For the composite structure with X = 135nm, the resonant mode shifts to 567 nm as shown in Fig. 3(c), and the corresponding electric field intensity distribution of the resonant mode is shown in Fig. 3(f). In this mode, the electric field is primarily localized at the aperture edge near the groove, which is similar to the field distribution of a dipole. As shown in these three structures, all the periodic units are symmetric to the center of the apertures in the *x*-direction, regardless if gratings are added into the aperture arrays. As a result, their electric field distributions are also symmetric to the center of the holes, leading to a single resonant dip in the reflection spectra.

#217826 - $15.00 USD Received 25 Jul 2014; revised 5 Oct 2014; accepted 8 Oct 2014; published 14 Oct 2014
(C) 2014 OSA

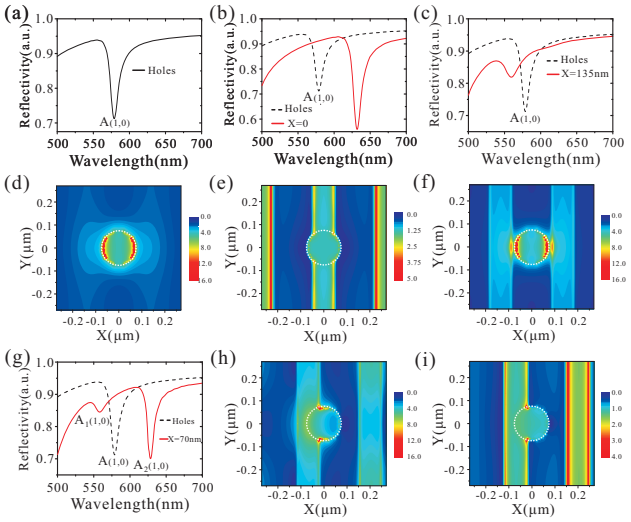

Fig. 3. (a) The reflection spectrum of the aperture array and (d) its electric field intensity distribution at the resonant wavelength of 575 nm. (b) The reflection spectrum of the composite structure with X = 0, and (e) its field intensity distribution at 632 nm. (c) The reflection spectrum of the composite structure with X = 135 nm, and (f) the electric field intensity distribution at 567 nm. (g) The reflection spectrum of the composite structure with X = 70 nm. The electric field intensity distribution of the $A_1(1,0)$ and $A_2(1,0)$ resonant modes is shown in (h) and (i) respectively. In all field distributions, the dashed white rings represent the aperture position.

We now examine cases with two resonant modes. Figure 3(g) shows the calculated reflection spectrum of the composite structure with X = 70nm, while the electric field intensity distribution of mode $A_1(1,0)$ and $A_2(1,0)$ are shown in Figs. 3(h) and 3(i), respectively. For the $A_1(1,0)$ mode, the electric field is primarily distributed in the region where the aperture and groove overlap, especially at the intersections of the structure edges. However, for the $A_2(1,0)$ mode, the electric field is primarily distributed at edge of the neighbouring groove. In such composite structures with X between 0 and 135nm, the structure symmetry is broken. Thus, the basic resonant mode splits into two modes, which correspond with the two dips in the reflection spectra.

3. Experimental demonstration and tuning of the optical properties in the composite structures

Next, we experimentally demonstrate the optical properties in the composite structures. After a 100 nm thick silver film is deposited onto the silicon substrate via magnetron sputtering, the nano-structures are fabricated on the silver film by focus-ion-beam milling (FIB, Helios Nanolab 600i). Figures 4(a)-4(f) show the scanning electron microscopy (SEM) images of our samples with different X, where all geometric parameters, except X, are the same as those in simulation. Then the reflection spectra are measured via an ultraviolet-visible-near-infrared microspectrophotometer (CRAIC QDI2010) with a halogen lamp as the light source. Figures 4(g) and 4(h) show the measured reflection spectra under normal incidence of TM and TE light, respectively. Compared with the reflection spectra in Figs. 2(b) and 2(c), the experimentally measured results agree with the calculated results in both the resonant position and wavelength shift trend. By changing the relative displacement X, both the resonant wavelength and the number of resonant modes can be simultaneously tuned under TM polarized illumination.

#217826 - $15.00 USD Received 25 Jul 2014; revised 5 Oct 2014; accepted 8 Oct 2014; published 14 Oct 2014
(C) 2014 OSA

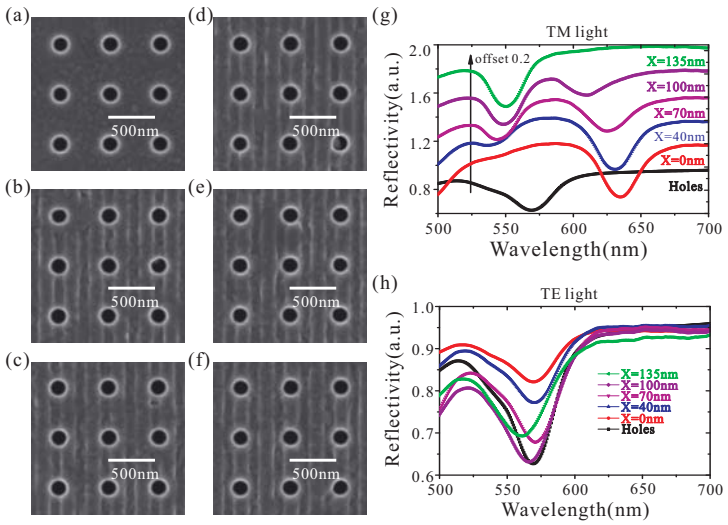

Fig. 4. The SEM images of the (a) apertures as well as the composite structures with (b) X = 0, (c) X = 40 nm, (d) X = 70 nm, (e) X = 100 nm and (f) X = 135 nm. The measured reflection spectra of these structures under normal (g) TM and (h) TE light.

Because the composite structures in our design are sensitive to the geometric parameters, we can tune their optical properties by varying specific parameters. In the discussions above, we see that the optical properties can be tuned by changing the relative displacement X between the aperture arrays and the gratings. We now focus on another parameter: the groove depth *h*. Figure 5(a) shows the calculated wavelength shift of the resonant dips for variations in *h* between 10nm and 30nm, while Fig. 5(b) shows the experimental resonant wavelength shifts. We can see that the experimental results reasonably agree with the calculated ones. For the X = 0 case, the deeper groove introduces a red shift. However, for the X = 135 nm case, deeper groove introduces a blue shift. For cases with two resonant modes, the deeper groove leads to a blue shift for mode $A_1(1,0)$ and a red shift for mode $A_2(1,0)$. Thus, the groove depth *h* can also be used to tune the resonant wavelength of the mode. In this way, the SP resonances in this composite nanostructure can be significantly modulated by changing the geometric parameters, such as the relative positions between nanoaperatures and gratings, and also the groove depth. Based on these principles, the present composite metallic aperture array may have potential applications on some tunable optodevices, such as subwavelength sensors and detectors.

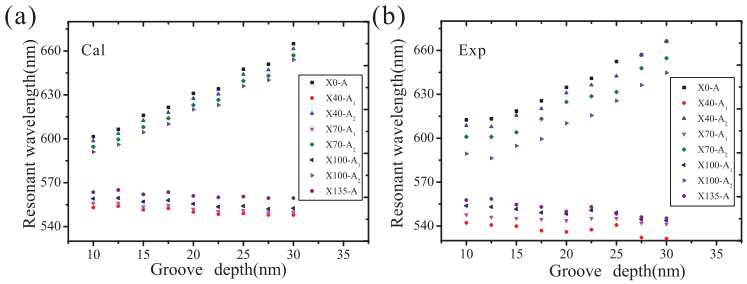

Fig. 5. The (a) calculated and (b) experimental resonant wavelength for different groove depth.

4. SPs propagation in the composite structures

Now that the excitation and the propagation of SPs significantly influence the optical properties of the composite nanostructure, it is worthwhile to track the in-plane propagation of SPs in the nanostructures. Actually for SPs propagating on the surface of the flat silver film, the electric

#217826 - $15.00 USD Received 25 Jul 2014; revised 5 Oct 2014; accepted 8 Oct 2014; published 14 Oct 2014
(C) 2014 OSA

field intensity decays exponentially along the propagation direction. Figures 6(a) shows the silver film in our simulation, where the boundary conditions are set perfectly matched layers (PMLs) in both *x*- and *z*-direction, periodic boundary conditions are used in *y* direction to represent an infinite region, and the source is selected mode source to simulate SPs plane waves. The calculated propagation processes are shown in Figs. 6(b)-6(d), for the electric field intensity distributions at different wavelengths. The SPs on the flat metal-dielectric interface [3,9] cannot interact with the incident light due to the mismatch of momentum, and they decay exponentially with the propagating distance, and the intrinsic loss decreases as the wavelength increases.

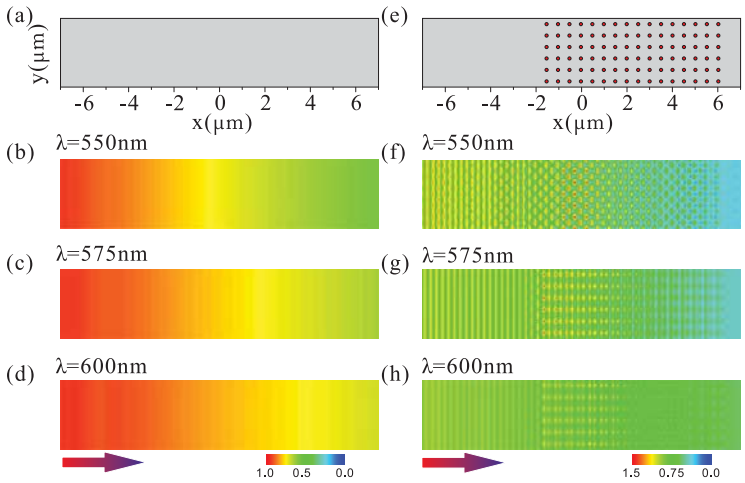

Fig. 6. (a) The schematic of the flat silver film, and (b) - (d) The SP propagation processes along the film surface at wavelengths of 550 nm, 575 nm, and 600 nm, respectively. (e) The flat silver film with the aperture array. (f) - (h) The SPs propagating along the surface at 550 nm, 575 nm, and 600 nm, respectively.

The SPs on the structured surface is intrinsically different from those on the above flat interface. Once periodic nanostructures contribute the reciprocal lattice vectors and provide additional momentum, the SPs can interact strongly with the incident light due to the momentum matching between them [3, 4, 14]. Consequently, the SP polaritons are excited at resonant frequencies and propagate along the nanostructured surfaces. Generally, all these waves that propagate along the metal-dielectric interface are called as SPs [3]. To explore all these SPs propagation properties in the composite structures, we apply this simulation on the composite nanostructures described in Sec.2 and Sec.3. For example, Fig. 6(e) schematically shows the aperture array in our simulation, and the corresponding propagation processes of SPs are described in Figs. 6(f)-6(h). Compared with Figs. 6(b)-6(d), the SP propagation process is quite different from that on the flat film and the in-plane transmitted field intensity becomes weaker because of scattering of the aperture array. For short wavelength region such as 550nm (as shown in Fig. 6(f)), the intrinsic loss in the silver film is large. The SPs are severely scattered by the apertures, and little energy propagates through the aperture array. At the resonant wavelength of 575 nm (as shown in Fig. 6(g)), the intrinsic loss become lower, however, the scattering energy is largely enhanced because of the resonance, and the dipole-like field is localized in the apertures. Further, in Fig. 6(h) for 600 nm, the intrinsic loss and scattering are greatly reduced and little field is localized in the apertures, leading to an increase in the in-plane transmitted energy.

Then we experimentally measure the energy transmitted through the structures. In our experiment, a supercontinuum laser (Fianum, SC400) is used as the excitation source, and the far-field images are captured with a CCD. Figure 7(a) shows two of the samples we used, one is

#217826 - $15.00 USD Received 25 Jul 2014; revised 5 Oct 2014; accepted 8 Oct 2014; published 14 Oct 2014
(C) 2014 OSA

a flat silver film with two grooves, while the other sample contains an aperture array with two grooves in the silver film. One of the parallel grooves is fabricated to couple the free-space light in order to launch SPs, while the other groove is used to scatter the SPs into the free space. We present the captured images of both the flat film and the aperture array at different wavelengths in Figs. 7(b)-7(d). In the flat silver film sample, the SPs can propagate on the silver film in a wide wavelength range. For the samples with either aperture arrays or composite structures, the propagation processes are greatly modified. For the short wavelength region shown in Fig. 7(b), the intrinsic loss of silver is large. The SPs are severely scattered, and there is little light out coupling. At the resonant wavelength of 575 nm shown in Fig. 7(c), the scattering light in the aperture array is obviously increased. For the long wavelength region shown in Fig. 7(d), the scattering as well as the intrinsic loss is decreased, so the light out-coupling is obviously increased.

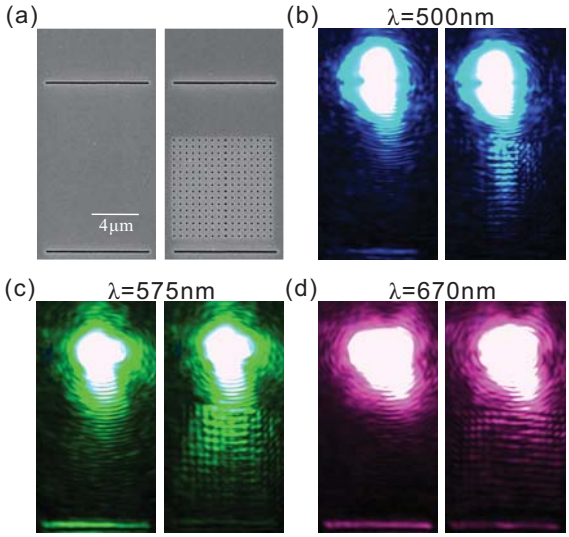

Fig. 7. (a) The SEM images of representative samples. The sample on the left consists of two parallel grooves in the silver film, with 8.64μm lengths and 14.3μm spacing. The sample on the right consists of an aperture array between two parallel grooves, with an array region of 8.64 x 8.64μm ^{2}. (b) - (d) Experimental CCD images under excitation wavelengths of 500 nm, 575 nm and 670 nm, respectively.

To have a clearer understanding of the SP in-plane propagation properties of different structures, we have collected the transmitted field intensity at different wavelengths, under the same simulated and experimental conditions as those used in Figs. 6(a) and 7(a). Here, we define the propagation coefficient to characterize the in-plane transport of the SPs as follows: $T_{rel} = T_s / T_0$,where T_S is the intensity of electric fields propagating through the structures (within the plane), and T_0 is the intensity of electric fields propagating through the flat silver film (within the plane). The propagation coefficients corresponding to different wavelengths are shown as square black dots in Figs. 8(a)-8(d). The experimental propagation coefficients, which are obtained by using the out-coupled light intensity from the groove, are also shown as red stars in Figs. 8(a)-8(d). These results are well matched with each other, especially for long wavelengths. Because short wavelength scattering is strong, it significantly influences the detection in our experiments, reducing the precision of the measured out coupled field energy. However, the experimental results can still correctly describe the physical process, because they agree with the actual propagation process in simulation. In this way, we have studied the SP propagation properties using far-field experiments. Unlike previous observational

#217826 - $15.00 USD Received 25 Jul 2014; revised 5 Oct 2014; accepted 8 Oct 2014; published 14 Oct 2014
(C) 2014 OSA

measurements in far field experiments, we offer a semi-quantitative measurement method using CCD to “record” the SP propagation.

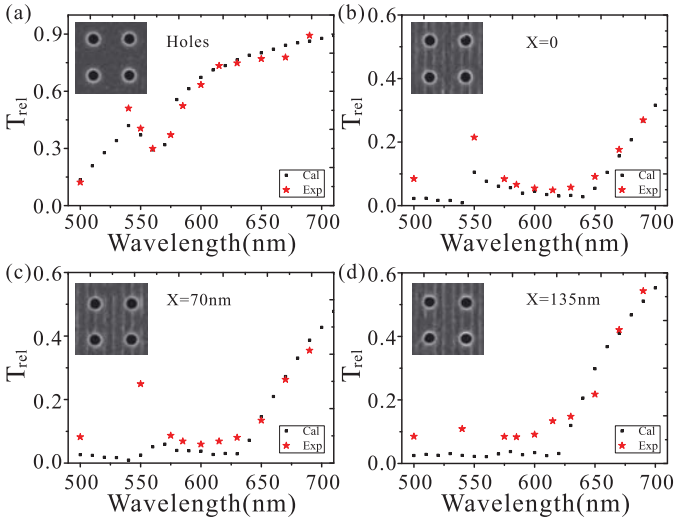

Fig. 8. The in-plane propagation coefficients of (a) the aperture array as well as composite structures with (b) X = 0, (c) X = 70 nm and (d) X = 135 nm.

As we know, the experimentally measured spectra of the composite nanostructures show reflection dips at resonant wavelengths, as shown in Fig. 4(g). Here the CCD images actually describe the specific in-plane propagating properties at the same wavelengths (in Fig. 7), resulting in low propagation coefficient at those wavelengths (in Fig. 8). At these resonant wavelengths, the propagating SPs mode can be effectively converted to free-space light, leading to the resonant dips in the reflection spectra and small propagation coefficients of SP transport. In this way, we obtain the physical consistency from all the previous results.

5. Conclusion

We have theoretically and experimentally studied the optical properties of composite nanostructures with aperture arrays and gratings. Under normal TM light illumination, the resonant modes of the aperture arrays can be modified by adding gratings. Once the symmetry of the periodic unit is broken, the resonant mode splits into two modes. Moreover, the resonant wavelengths of the composite structures can be effectively tuned by geometric parameters such as the relative displacement X and the groove depth *h*. Therefore, these composite nanostructures may have potential applications on some tunable optodevices, such as subwavelength sensors and detectors. However, under normal TE light illumination, only a slight wavelength shifts occur at the resonant mode.

We then studied the SP in-plane propagation properties in composite structures. The propagation coefficient we defined can be used to characterize the in-plane transport of the SPs, and the lowest in-plane propagation coefficients correspond with the dips in the reflection spectra at normal illumination. Moreover, the experimental propagation coefficients agree with the calculated ones. As a result, our method offers a convenient way to study the SP propagation properties using far field experiments.

Acknowledgments

This work was supported by the Ministry of Science and Technology of China (Grant Nos. 2012CB921502 and 2010CB630705), and the National Natural Science Foundation of China (Grant Nos. 11034005, 11474157, 61475070, 11321063, and 91321312).

#217826 - $15.00 USD Received 25 Jul 2014; revised 5 Oct 2014; accepted 8 Oct 2014; published 14 Oct 2014
(C) 2014 OSA